Quantum interference in two-photon spectroscopy for laser stabilization and cesium-cell comparison

Chien-Ming Wu,[1,3] Tze-Wei Liu,[1,2,3] and Wang-Yau Cheng[3,*]

[1]*IAMS, Institute of Atomic and Molecular Science, Academia Sinica, Taiwan*

[2]*Taiwan International Graduate Program in Molecular Science and Technology Program, National Central University and Academia Sinica, Taiwan*

[3]*Physical Department, National Central University, Taiwan*

(Received 9 April 2015; published 9 October 2015)

An alternate method of two-photon spectroscopy is presented where cesium atoms interact with a phase-modulated laser beam. Doppler-free two-photon spectroscopy of the cesium atom $6S \rightarrow 8S$ hyperfine transition was used to experimentally demonstrate quantum interfered two-photon spectra. We calculated the photon-atom interaction by second-order perturbation theory and assumed that the one-photon frequency is detuned far from any intermediate state. Then we calculated the relative transition rates of all spectral lines resolved by the laser carrier and sidebands. A physical picture of multipathway quantum interference in the frequency domain is given that explains the unusual line strength, based on the trick that a phase-modulated laser beam can be decomposed into a series of coherent and collinear laser modes (carrier and sidebands). For all pairs of modes in which the sum frequency of each pair was on resonance with the cesium atom $6S \rightarrow 8S$ transition, the superposition of all pathways induced by the different mode pairs resulted in a destructive interference, which then leads to a lack of absorption. We have shown in this paper that our calculation agrees very well with our experimental results in terms of the relative interfered line strengths, which were functions of modulation depth. We further discuss some related issues concerning laser stabilization and we demonstrate an approach for simultaneously comparing two cesium cells.

DOI: 10.1103/PhysRevA.92.042504 PACS number(s): 32.30.−r

I. INTRODUCTION

High-resolution laser spectroscopy plays a key role in the recent advances in both fundamental physics [1] and metrology applications [2]. In particular, the measurement of an atomic transition frequency via a high-resolution spectrum is the most important part in establishing reliable optical frequency standards, either primary or secondary [3]. In 2013, one special scheme for two-photon spectroscopy was employed by Wu *et al.* in which an unperturbed two-photon spectrum of the cesium atom $6S$-$8S$ transition was accurately resolved [4]. The key technique used in that study [4] involved a unique quantum interfered two-photon spectrum that allowed for offset locking of the laser frequency. Quantum interference in atomic two-photon spectroscopy has been studied under two different physical situations where pulse lasers were employed: One focused on wave function overlapping in the time domain that is analogous to two-slit interference in the spatial domain [5]; another emphasized multipathway interference resulting from a "cross damping" phenomenon [6]. In this paper, we present a special physical situation other than the aforementioned two cases since we consider the effect of a phase-modulated continuous wave on the photon-atom interaction. We studied both theoretically and experimentally how a phase-modulated laser beam can disturb the two-photon transition probability and the related applications to laser stabilization. We also demonstrated a high-precision comparison between two cesium cells by using the "crossover" line in the interfered two-photon spectrum.

II. TWO-PHOTON SPECTRUM INTERFERED WITH BY PHASE-MODULATED LIGHT

The upper part of Fig. 1 displays our experimental setup to obtain the unique cesium $6S$-$8S$ two-photon spectrum that was resolved by the phase-modulated light. The lower part of Fig. 1 shows the relevant energy level diagram. A single-mode, linearly polarized laser beam was first passed through an electro-optical modulator (EOM), The beam was then split by a glass plate and sent into the following two areas of interest: A small portion of the laser light was sent to the area including a scanning Fabry-Perot (FP) system to record the intensity distribution between the carrier and sidebands. The rest of the laser light was sent to the area including a cesium cell and was retroreflected back. A near-perfect beam overlap was realized by using a power meter (see Fig. 1) to detect the power of the retroreflected laser beam that actually passed through the same spatial filter twice [4,7]. The linewidth of our home-built FP was 2.52 MHz. The EOM was phase modulated with 106 MHz modulation frequency (Ω); that is, the light phase ϕ was modulated by $M \cos \Omega t$, where the modulation depth M was variable in our experiment. The electric field after the EOM in Fig. 1 can be expressed in the form of Bessel function identities:

$$\begin{aligned} E &= E_0 \cos(\omega_c t + M \cos \Omega t) \\ &= E_0 \sum_{n=-\infty}^{n=\infty} (-1)^n J_n(M) \cos(\omega_c + n\Omega)t, \end{aligned}$$

where ω_c stands for the laser carrier frequency and $J_n(M)$ denotes the nth Bessel function. A Doppler-free two-photon spectrum was achieved by using two quarter-wave plates $(1/4\lambda)$ since the $6S$-$8S$ two-photon transition that is not on resonance with any intermediate state can only occur when the left-circular polarized light and the counterpropagating

*wycheng@ncu.edu.tw

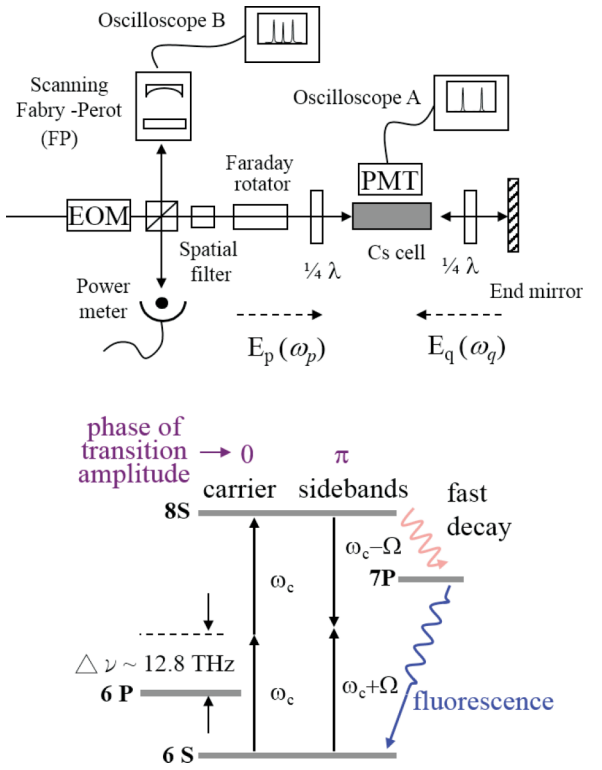

FIG. 1. (Color online) Experimental setup for resolving the two-photon interfered spectrum and the relevant level diagram of the cesium atom for illustrating the two-pathway interference. 1/4 λ: quarter-wave plate; E_p (E_q): electric field of forward (retroreflected) laser beam; PMT: photon-multiplier tube; FL: fluorescence. For other symbols in the diagram, see text.

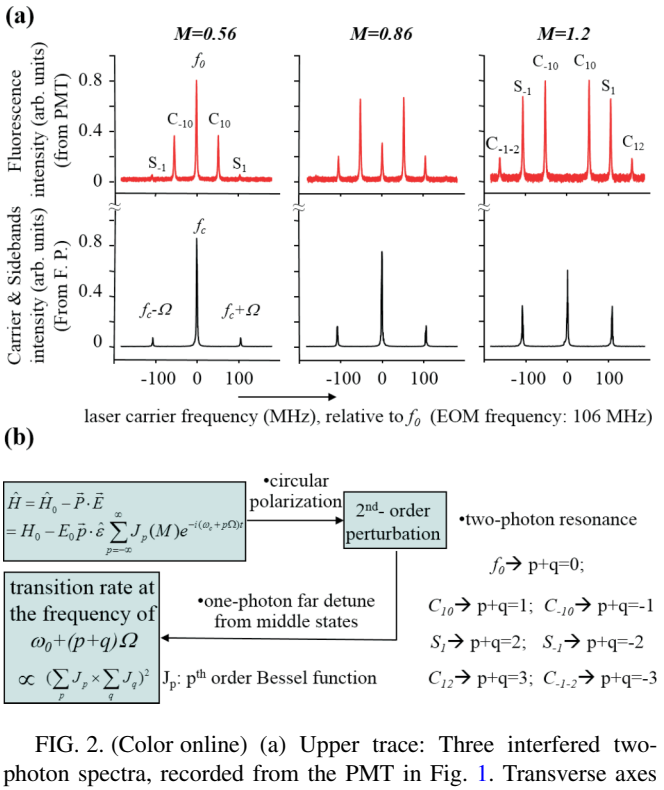

FIG. 2. (Color online) (a) Upper trace: Three interfered two-photon spectra, recorded from the PMT in Fig. 1. Transverse axes are the laser carrier frequency, relative to the cesium atom $6S$-$8S$, $F = 4 \rightarrow F' = 4$ two-photon resonant frequency (f_0). Note that the f_0 line is missing when the modulation depth M is 1.2. Lower trace: Corresponding intensity distribution between carrier and sidebands, recorded from the Fabry-Perot in Fig. 1. (b) Left side: flow chart of our theoretical treatment for calculating the relative transition strength of each line in (a); right side: the corresponding $p + q$ for each line; p, q are all integrals; see text.

right-circular polarized light interacted with the same atoms. In other words, no evidence of a two-photon transition was found when a unidirectional and circular-polarized laser beam was employed. This was the main mechanism leading to the nearly complete removal of the Doppler background in the two-photon spectrum of Fig. 2. To theoretically analyze the spectrum obtained from the photon-multiplier tube (PMT) of Fig. 1, one can start from second-order perturbation theory [6,8,9] with the addition of γ_n as the population decay rate of level n; that is,

$$\left[\frac{d}{dt} + \pi\gamma_f\right] a_f^{(2)}(t) = \frac{1}{i\hbar}\sum_m a_m^{(1)}(t) p_{mf} E_q e^{-i\omega_{mf}t} \quad (1)$$

and

$$a_m^{(1)}(t) = \frac{-1}{i\hbar}\sum_p \frac{p_{mg}E_p}{(\pi\gamma_m) + i(\omega_{mg} - \omega_p)} e^{i(\omega_{mg}-\omega_p)t}, \quad (2)$$

where $a_m^{(1)}(t)$ gives the probability amplitude that corresponds to first-order perturbation of the wave function and m represents all the intermediate states. Similarly, $a_f^{(2)}(t)$ stands for the probability amplitude that corresponds to second-order perturbation and f denotes the final state (the $8S$ energy level in our case). Some symbols in Eqs. (1) and (2) are as follows: $p_{mf}E_q \equiv \langle m|\vec{p}\cdot\hat{\varepsilon}|f\rangle E_q$ gives the dipole transition amplitude with transition frequency ω_{mf} where m and f denote the unperturbed eigenstates $\langle m|$ and $|f\rangle$, and p stands for the induced dipole moment and $\hat{\varepsilon}$ stands for the unit vector in the direction of the electric field; ω_{mg} is the transition frequency from the intermediate state $|m\rangle$ to the ground state $|g\rangle$; the electric field $\vec{E} = E\hat{\varepsilon}$ is phase modulated and can be viewed as a superposition of different frequency components $\vec{E}_p(\omega_p)e^{-i\omega_p t}$ as

$$\vec{E} \equiv E_0\hat{\varepsilon}e^{-i(\omega_c t + M\sin\Omega t)} = \hat{\varepsilon}\sum_p E_p(\omega_p)e^{-i\omega_p t}$$

$$= E_0\hat{\varepsilon}\sum_{p=-\infty}^{\infty} J_p(M)e^{-i(\omega_c + p\Omega)t}, \quad (3)$$

where p is an integer and $\omega_p \equiv \omega_c + p\Omega$. Note that we have applied the boundary condition for the equation $a_m^{(N)}(t)$ as $a_m^{(N)}(t \rightarrow -\infty) = 0$ and have also made use of the fact that, in our experiment, the upper-level saturation due to two-photon absorption was too weak to be observed. Therefore, second-order perturbation theory was suitable in our case. From Eqs. (1) and (2) one can obtain the two-photon transition amplitude $a_f^{(2)}(t)$ as

$$a_f^{(2)}(t) = \frac{1}{\hbar^2}\sum_{p,q}\frac{1}{(\pi\gamma_f) + i(\omega_{fg} - \omega_p - \omega_q)} e^{i(\omega_{fg}-\omega_p-\omega_q)t}$$

$$\times \sum_m \frac{p_{fm}E_p p_{mg}E_q}{(\pi\gamma_m) + i(\omega_{mg} - \omega_p)}, \quad (4)$$

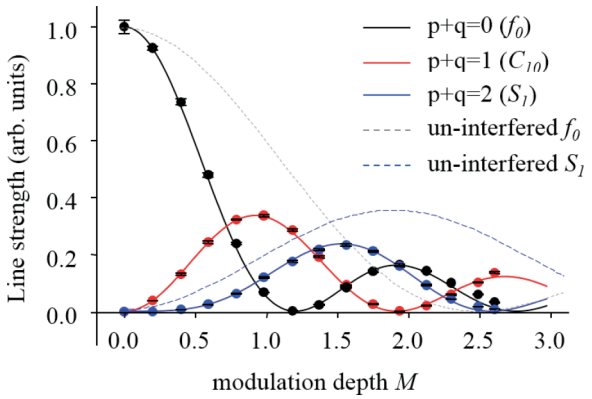

FIG. 3. (Color online) Line strength (proportional to $a_f^{(2)} a_f^{(2)*}$) of different $p+q$ values versus modulation depth (M), where p, q are integers; see text. Solid dots are experimental data with error bar. The first four orders of Bessel function were employed for the theoretical curve (solid line).

where $\omega_q \equiv \omega_c + q\Omega$, $p_{fm} = \langle f|\vec{p}\cdot\hat{\varepsilon}_p|m\rangle$, and $p_{mg} = \langle m|\vec{p}\cdot\hat{\varepsilon}_q|g\rangle$.

We now note that in our experiment (i) $\hat{\varepsilon}_p$ was left circular polarized and $\hat{\varepsilon}_q$ was right circular polarized. In other words, a two-photon transition would not occur with any unidirectional beam. (ii) $\omega_{mg} - \omega_p$ ($\sim$12.8 THz) $\gg \Omega$ (106 MHz), which means that the frequency detunings to intermediate states for carrier and all sidebands could be treated the same. (iii) We focused only on the case that $\omega_{fg} - \omega_p - \omega_q = 0$, that is, $\omega_{fg} - 2\omega_c - (p+q)\Omega = 0$.

Therefore, the second-order transition probability in Eq. (4) can be expressed in a much simpler form as

$$a_f^{(2)} a_f^{(2)*} = \alpha I_p I_q' \left(\sum_p J_p \times \sum_q J_q \right)^2, \qquad (5)$$

where $\alpha = [\frac{1}{\hbar^2(\pi\gamma_f)} \sum_m \frac{p_{mg}\, p_{fm}}{\pi\gamma_m + i(\omega_{mg} - \omega_p)}]^2$, $I_p = (E_0 E_0^*)_{\text{forward}}$, and $I_q' = (E_0 E_0'^*)_{\text{retroreflected}}$.

Equation (5) is used to explain the spectrum in Fig. 2 and the fitting curves in Fig. 3. When $p+q=0$, that is, $\omega_{fg} = 2\omega_c$, the values of (p,q) can be (0,0), (1,−1), (2,−2), etc. The strength of the $f_0(M)$ line in the spectrum of Fig. 2 is then proportional to $I_p I_q' (J_0^2 - 2J_1^2 + 2J_2^2 - 2J_3^2 + 2J_4^2)^2$ based on Eq. (5) and on the fact that $J_p = (-1)^p J_{-p}$, where we dropped all other terms including $|p| > 4$ and $|q| > 4$. Similar arguments can be applied to the C_{10} (crossover) line and the S_1 line in Fig. 2, which matched the conditions of $p+q=1$ and $p+q=2$, respectively. That is, the line strength of the $C_{10}(M)$ line is proportional to $I_p I_q' (2J_0 J_1 - 2J_1 J_2 + 2J_3 J_2 - 2J_3 J_4)^2$ under the condition that the laser carrier frequency ω_c is equal to $(\omega_{fg} + \Omega)/2$; the line strength of $S_1(M)$ is proportional to $I_p I_q' (2J_0 J_2 + J_1^2 - 2J_1 J_3 + 2J_2 J_4)^2$ under the condition that the laser carrier frequency $\omega_c = (\omega_{fg} + 2\Omega)/2$. Figure 2 presents the observed spectrum, in which all lines actually result from the same cesium two-photon transition, namely, the transition from the ground-state hyperfine level $6S$, $F = 3$ to the upper hyperfine level $8S$, $F' = 3$. Note that the term "crossover" has a different physical meaning from that commonly used in saturation spectroscopy. For example, the C_{10} line is resolved when all the atoms, including zero-velocity atoms, are involved in the absorption (first-order Doppler-effect approximation). This is very different from the concept of crossover in saturation spectroscopy in which the atoms of a certain velocity saturate the absorption. The upper trace in Fig. 2(a), recorded by the PMT and displayed on the oscilloscope A in Fig. 1, shows different spectra at different modulation depths M [$\phi = M\cos\Omega t$, Eq (1)]. The intensity distribution between carrier and sidebands, recorded by oscilloscope B in Fig. 1, is shown under each corresponding spectrum. One interesting feature in the spectra of Fig. 2(a) is that the f_0 line disappeared at $M = 1.2$, even though oscilloscope B showed that the intensity of the carrier was still larger than all the sidebands. How can a light beam, once it is phase modulated, become invisible to atoms and thus free from being absorbed? This was not easy to comprehend from a time-domain picture, but a simple explanation using frequency domain analysis is illustrated by the level diagram in Fig. 1, from which we can treat the photon-atom interaction approximately like a "two-pathway" interference process. In other words, in terms of the transition amplitude $a_f^{(2)}(t)$, the property $J_p = (-1)^p J_{-p}$ of Bessel functions always leads to a π-phase difference between the two transition pathways which result from the (ω_c, ω_c) photon pair and from the $(\omega_c + \Omega, \omega_c - \Omega,)$ photon pair. At a modulation depth (M) of 1.2, complete destructive interference occurs since $J_0^2(M) - 2J_1^2(M) \sim 0$. Figure 3 confirms Eq. (5) quantitatively, since the experimental data are in very good agreement with the theoretical curves for the f_0, C_{10}, and S_1 lines. The dashed lines in Fig. 3 are the predicted line strengths of uninterfered spectra resolved by the carrier and first sideband, respectively. We notice that the first interfered crossover line (C_{10}) needed much less modulation to achieve the maximum line strength compared with that of the first uninterfered sideband (S_1). This fact makes laser stabilization much more convenient, as will be discussed in more detail in the next section.

III. LASER STABILIZATION AND COMPARISON OF CESIUM CELLS

An interesting feature presented in both Figs. 2(a) and 3 is that the C_{10} (or C_{-10}) line intensity increased with increasing modulation depth M much faster than the other lines, which is very useful for laser frequency offset locking. The first-derivative-like spectrum for laser stabilization to the C_{-10} line was retrieved from a lock-in amplifier under the situation that the laser modulation frequency Ω was intentionally dithered by $A\sin\omega_m t$, that is,

$$\phi = M\cos(\Omega + A\sin\omega_m t)t; \qquad (6)$$

that is, the sidebands were dithered with a dither frequency ω_m. Note that the carrier frequency was not dithered and each $\pm N$ sideband pair was dithered in opposite phase; hence, no corresponding derivative signal at the spectral position of $p+q=0$ (f_0 line) was found. In other words, taking the +1 and −1 sideband pair as an example, at the moment when the +1 sideband was dithered to the maximum frequency $\omega_c + \Omega + A$, the −1 sideband would be dithered to its minimum frequency $\omega_c - \Omega - A$, which results in zero dither at the sum frequency of $2\omega_c$. Therefore, the ±1 dithered sideband pair would not cause any intensity modulation of fluorescence on

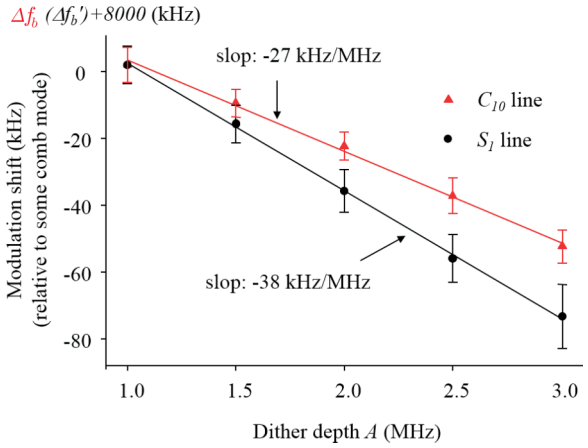

FIG. 4. (Color online) Modulation shift versus dither depth. The C_{10} line yielded a smaller modulation shift than the S_1 line. Δf_b ($\Delta f_b'$): the beat-note frequency between the CW laser and one comb mode of comb laser. $\Delta f_b = \Delta f_b' + \Omega/2$ (Ω: EOM frequency).

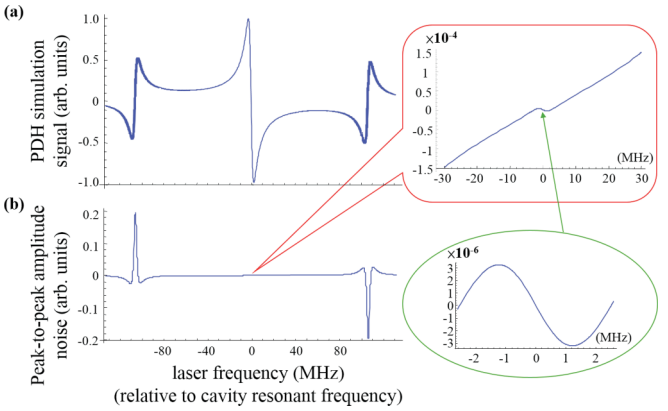

FIG. 5. (Color online) (a) The normalized dispersion-phase PDH signal with dithered sideband in which the following parameters are used for the simulation: EOM modulation frequency: 106 MHz; dither frequency: 27 kHz; optical dither width: 2 MHz; modulation depth: 0.4; cavity linewidth: 2.52 MHz. (b) The peak-to-peak amplitude noise of the PDH signal that was extracted from (a) by an undithered PDH signal. Note that this noise is smaller than 3×10^{-4} of the PDH signal height (red inset) when the laser frequency was detuned by less than 30 MHz from the cavity resonance frequency. This noise even has an order of magnitude of 6×10^{-6} when the laser frequency was tuned to differ from the resonance frequency by less than 2 MHz (green inset)

the f_0 line and hence no error signal from the lock-in output at the spectral position of $p + q = 0$ (f_0 line). Furthermore, locking the laser frequency to the C_{10} (or C_{-10}) line has three advantages. First, the frequency of the unmodulated laser beam before the EOM could be precisely controlled by simply changing the modulation frequency Ω on EOM. In our case, a proton-exchange MgO-doped $LiNbO_3$ based fiber EOM was used [10]. Thus the laser carrier frequency could be precisely adjusted to anywhere within a ± 10 GHz offset from the frequency of the C_{10} (or C_{-10}) line, while keeping the laser frequency at 1 kHz instability (30 s time constant) and 10 kHz accuracy. Later in this paper we will demonstrate a comparison of high-precision, unperturbed spectra by taking advantage of this technique. The second advantage is that one does not need a large modulation depth (M) to obtain an adequate signal-to-noise ratio (S/N) for optical offset locking. This has been proved in Figs. 2(a) and 3, which show that a small modulation ($M = 0.56$) can yield a C_{10} line with ten times larger S/N than that of the S_1 line. This is enough for laser stabilization at 30-mW total laser power. Furthermore, to achieve maximum S/N, Fig. 3 shows that the C_{10} line (red curve) only needs half as much modulation depth compared with that needed for the uninterfered sideband (S_1). As the third advantage, the C_{10} line suffers less modulation shift [11] since the carrier frequency was not modulated. This is confirmed by the experimental data in Fig. 4 where the modulation shifts were measured by frequency beating with a self-reference comb laser. For easy comparison of the slopes of the shifts, we put the two lines to be displayed in one chart in Fig. 4, though the spectral positions of the two lines are actually separated by half of the EOM frequency ($\Omega/2$). Besides the modulation shift, the light-shift effect is often discussed in two-photon transitions [12]. We were wondering if different scales of quantum interference, under the same total laser power, would yield the same light shift or not? Since different modulation depths will lead to different scales of quantum interference, as illustrated in Figs. 2 and 3, an examination of the light shift under different modulation depths (M) was performed. We varied the modulation depth at a fixed total laser power and observed the frequency difference between the f_0 and C_{10} lines (labeled as $\Delta f_0 C_{10}$). No obvious change of $\Delta f_0 C_{10}$ was perceived under different modulation depths or different scales of quantum interference. The equal light shift of the f_0 and C_{10} lines, in spite of their very different transition amplitudes, implies that the effect of light shift depends only on the total laser power and not on the individual line strengths, if the frequency detunings to the intermediate states are considered to be the same [12]. This observation confirms the assumption used to derive Eq. (5), in which the carrier and all sidebands were considered to have nearly the same frequency detuning from the intermediate states.

The EOM in Fig. 1 was not only used for stabilizing the laser and for freely adjusting the laser absolute frequency, but also permitted narrowing the laser linewidth by using a reference cavity. One question may arise whether the Pound-Drever-Hall (PDH) curve used for the laser stabilization would be distorted as the frequencies of the sidebands were dithered. The answer would be no if the laser carrier frequency was stabilized to the center of the dispersion phase of the PDH signal. However, the answer would be yes if the laser carrier frequency was detuned too far from the cavity resonant frequency. In Fig. 5(a), a simulation up to the first sideband was performed to illustrate the influence on the PDH profile under the condition that the EOM sidebands were dithered in the way indicated by Eq. (6), using the experimental conditions listed below: 106-MHz EOM modulation frequency (Ω); 1360-MHz cavity free spectral range with a finesse of 540; 27-kHz sideband dithering frequency (ω_m) with the resulting optical dither range of 2 MHz ($2A$), where the symbols in parentheses are those used in Eq. (6). The simulation in Fig. 5(a) is actually a plot of Im $[F(\omega)F^*(\omega + \Omega) - F^*(\omega)F(\omega - \Omega)]$ [13], where $F(\omega) = (re^{i\Phi} - r)/(1 - r^2 e^{i\Phi})$ and Φ stands for the round-trip phase of light traveling in our 11-cm-long cavity; r stands

for the amplitude reflection coefficient of the cavity mirrors and is 0.994 in our case. One can find in Fig. 5(a) that the two sidebands of the PDH profile are seriously perturbed but the center of the PDH profile remains free from the dither. This is because the dither is canceled out at $\omega = 0$ where $F(0)F^*(\Omega)$–$F^*(0)F(-\Omega)$ equals zero at any modulation frequency Ω. Figure 5(b) shows the peak-to-peak residual of the PDH profile as a function of the laser frequency ω, from which one can understand that the PDH residual caused by sideband dither is only serious at frequencies around the sideband resonances. In another regime—for example, at ± 30 MHz detuning from the cavity resonant frequency, as illustrated in the red inset—the PDH residual was only 3×10^{-4} of the peak height of the PDH profile. The green inset in Fig. 5, magnified from the regime of ± 2 MHz detuning in the red inset, was almost free from the sideband dither with a residual smaller than 6×10^{-6} of the PDH signal.

Our previous investigations pointed out that the cesium atom $6S$-$8S$ transition was a good optical frequency reference due to its excellent spectral features [14]. The applications to Ti:sapphire comb lasers were also demonstrated [15,16] using a hand-size optical reference [17]. Therefore, further comparisons of the corresponding transition frequencies under different cell conditions are important and some comparisons were carried out in our previous experiment [4]. In this section, we use a more convincing experimental setup for the comparison of high-resolution spectra. In this study, an unmodulated laser beam was injected into a slave laser to build other similar cesium spectrometers, as shown in Fig. 6. This approach benefits from a simultaneous comparison between two cells, so that the influence of a common frequency offset from the master laser could be eliminated. We exchanged the two cesium cells after each measurement and that reduced some environmental errors. The reduction of the error budget is because the "real" frequency difference Δf_{real} of the two spectra is actually equal to the average of the measured frequency differences before exchanging the cells (Δf_m) and after exchanging the cells (Δf_m^{ex}). That is, $|\Delta f_{\text{real}}| = (|\Delta f_m| + |\Delta f_m^{ex}|)/2$, where $|\Delta f_m| = |\Delta f_{\text{real}}| + \Delta f$, $|\Delta f_m^{ex}| = |\Delta f_{\text{real}}| - \Delta f$, and $\Delta f (= \Delta f_L + \Delta f_{\text{PMT}} + \Delta f_B + \Delta f_{\text{misalign}} + \Delta f_{\text{2-order Doppler}} + \cdots)$ stands for the sum of the errors caused by the following facts: difference of the light shifts (Δf_L); different light responses of the PMTs (Δf_{PMT}); slightly different earth magnetic fields (Δf_B); frequency discrepancy caused by different precision of laser beam alignment ($\Delta f_{\text{misalign}}$) and the second-order Doppler shift ($\Delta f_{\text{2-order Doppler}}$) and so on. The light shift–caused error, which is generally the most troublesome issue in the frequency measurement of two-photon transitions [4,7,18,19], could be efficiently reduced by exchanging cells, if the power loss from the cell windows was measured beforehand. We quoted 2 kHz for the light-intensity-related error due to measurement uncertainty of the light scattering loss from the cell windows. A similar argument for the advantage of exchanging cells could also be applied to the reduction of errors coming from Δf_{PMT} and Δf_B and so on, in which the related errors were not perceived even when we replaced the PMT or removed the μ-metal from the cesium cell or intentionally misaligned the optical path. Note that we used the same high-voltage supply to provide the bias voltage of the two PMTs which

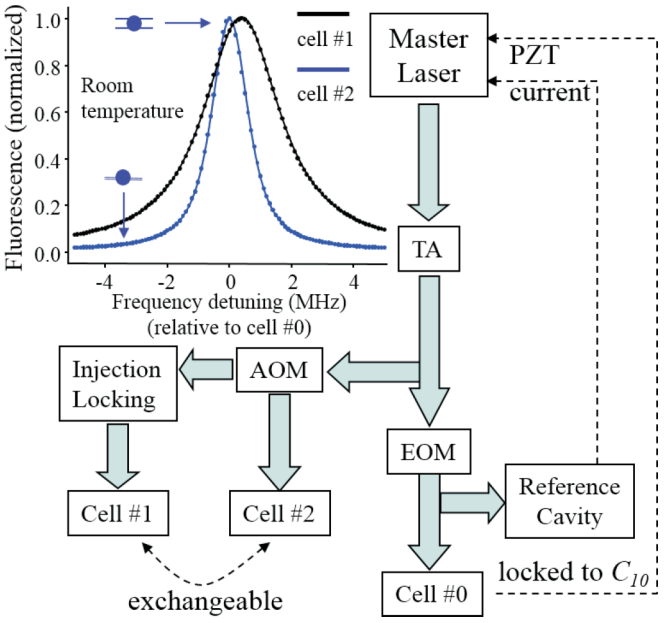

FIG. 6. (Color online) Block diagram for the comparison of cells and a typical simultaneously resolved spectrum (upper left), in which the black dots were obtained from cesium cell 1 while the blue dots were obtained from cesium cell 2. The error bar with its size relative to the corresponding dot is magnified and is pointed out by a blue arrow. TA: tapered amplifier. The transverse axis of the spectrum was the frequency relative to that resolved by cell 0 (see text). Cells 1 and 2 were exchangeable.

were installed in separate cesium-cell systems. When the two cells were exchanged, all the electronics for recording the spectral line shape remained unchanged. All the cells, except for cell 0 that was kept at 80 °C cell temperature, were at room temperature, so that the frequency error from pressure shift is ignorable since the cells were all in the same room which was temperature regulated with 1 °C uncertainty. Therefore, we could only evaluate the errors caused by the space-dependent discrepancies of the room temperature and the Earth's magnetic field according to the pressure-shift measurements in [4] and [19] and Zeeman-shift measurements in [4], and we concluded that those errors would not exceed 10 Hz. Uncertainty from line-shape fitting is 1.7 kHz for cesium cell 1 and 1.4 kHz for cesium cells 2 and 3. However, a statistical error of 9 kHz was found after scanning the spectrum nine times, and we suspect that some unknown optical interference associated with mirror mounts of different stability might cause the 9 kHz statistical errors in

TABLE I. Statistical and systematic uncertainties of the frequency difference in our experimental setup, in kHz.

Statistical	9
Measurement error on the light power scattered by cell windows	2
Electronics (including PMT bias voltage)	0.2
Different alignment for two optical paths	0.03
Difference of the Earth magnetic field	<0.01
Different collision shift (23 °C)	<0.002

TABLE II. Fitted transition frequency, relative to that of cell 0 (cell 0 at 80 °C; other cells at 23 °C).

$F = 4 \rightarrow F' = 4$	Frequency[a]	Linewidth[b]	Age[c]	Material
Cell 1 [7]	402 kHz	2.21 ± 0.02	>8	?
Cell 2 [4,20]	22 kHz	1.12 ± 0.010	5	Pyrex
Cell 3 [20]	23 kHz	1.08 ± 0.009	5	Pyrex

[a]12-kHz frequency uncertainty is quoted; see Table I for details. The average frequencies of cell 1 were the same when cell 2 was replaced by cell 3.
[b]In MHz, full width half magnitude.
[c]Years after purchasing.

the different light paths. Therefore, we quote a total 12-kHz error bar in our cell comparisons, as summarized in Table I.

Figure 6, upper left, displays one typical measurement result in which the two signal heights were normalized. The "cesium cell 1" in Fig. 6 was kindly provided by MPQ (Max Planck Institute for Quantum Optics) whose cesium cell was used in Ref. [5], and "cesium cell 2" was the local cesium cell that has been installed in our cesium spectrometer for the last 5 years. Another relatively new cesium cell from the same company as cesium cell 2 [20], labeled as cesium cell 3 and not shown in Fig. 6, was also put into comparison by replacing cell 2. The spectra were resolved point-by-point for nine times with a 100-kHz frequency interval per point and we took the average of nine scans to give the spectral positions and linewidths. The error bar of each point was smaller than the corresponding dot; hence it is magnified in Fig. 6 and is indicated by a blue arrow. The transverse axis in the upper-left spectrum of Fig. 6 is the frequency relative to the locking point of the aforementioned derivative signal resolved by cesium cell 0 [20]. An obvious difference between the two fitting peaks of cells 1 and 2 was found from the spectra and that difference remained unchanged even after we exchanged the two cesium cells. In other words, the frequencies of the two signal peaks still differed by 379 kHz, which is one order of magnitude greater than our measurement error (±12 kHz)! Note that the MPQ cell (cell 1) yielded a twice-wider linewidth than our local cell (cell 2), which was consistent with our previous observation [4], implying that the MPQ cesium cell might have changed with age by a long-term growth of residual gas or been contaminated during transportation [21]. Table II shows that the older cell (1) showed a serious frequency shift and broader linewidth, even though cell 1 had once been measured to have only 1.2-MHz linewidth by the Garching team 8 years ago [7]. Cell 2 had also been used in Ref. [4] and the linewidth was found to be the same as that of 2 years ago. Therefore, "collisions with residual gas" is the most probable cause for "aging" of the cell because collisions always bring about "collision shift" and "collision broadening" together [22], as we have found in Table II. Recently, Zamerosky *et al.* [23] further pointed out that the presence of helium gas diffused from the cell environment caused the frequency shift in our previous experiment of cesium-cell comparisons [4].

IV. CONCLUSIONS

We have presented a unique two-photon interfered spectrum that has been alluded to previously in the literature [4], but which is discussed here in detail. Thanks to the fact that the one-photon detuning is far enough from the intermediate states (12.8 THz, $6P_{3/2}$), the formulas for each line of the interfered spectrum could be simplified and experimentally confirmed. We found that, both theoretically and experimentally, the first interfered crossover resonance (C_{10}, C_{-10} lines) could greatly reduce the difficulties of applying high modulating voltage from EOM modulation if the intent was to perform optical offset locking, as demonstrated in this paper. We also show that the same EOM in our scheme could be multifunctional, that is, could be used for Pound-Drever-Hall (PDH) locking without losing the locking stability. We arranged a sophisticated optical layout for simultaneously comparing two cesium cells and we conclude that the $8S$ state cesium atoms are very sensitive to even tiny traces of residual gas. We believe that all the physics and techniques mentioned in this paper could be generalized to the fields of high-resolution nonlinear spectroscopy and ultrasensitive molecular cell comparisons. Ongoing works will include a similar setup for exploring cesium atom $6D_{5/2}$ and $6D_{3/2}$ states of which the corresponding two-photon spectra (884 nm) contain denser hyperfine lines and wider spectral range than our present works, offering more information for understanding the angular momentum–dependent hyperfine structure and hopefully offering more information on clarifying an interesting question of whether the frequency discrepancy of the two different cells observed in Fig. 6 is energy level dependent or not.

ACKNOWLEDGMENTS

We are grateful to Dr. Thomas Udem of MPQ for very helpful discussion and for suggesting the use of their cesium cell for comparison. Dr. Jon Hougen of NIST gave available comments about the "slit interference" analogy. Also, Dr. Yen-Chu Hsu in IAMS, Taiwan, supported studies in this report in many aspects that we very much appreciate. This research was funded by Ministry of Science and Technology Taiwan: MOST 103-2112-M-008-012.

[1] For example, Z.-T. Lu, P. Mueller, G. W. Drake, W. Nortershauser, S. C. Pieper, and Z.-C. Yan, Laser probing of neutron-rich nuclei in light atoms, Rev. Mod. Phys. **85**, 1383 (2013).
[2] H. S. Margolis, Frequency metrology and clocks, J. Phys. B **42**, 154017 (2009).
[3] F. Riehle, *Frequency Standards: Basics and Applications*, 1st ed. (Wiley-VCH, Weinheim, 2004); also see P. Gill, When should we change the definition of the second? Philos. Trans. R. Soc., A **369**, 4109 (2011).
[4] C.-M. Wu, T.-W. Liu, M.-H. Wu, R.-K. Lee, and W.-Y. Cheng, Absolute frequency of cesium 6S-8S 822 nm two-photon

transition by a high-resolution scheme, Opt. Lett. **38**, 3186 (2013).
[5] M. M. Salour, Quantum interference effects in two-photon spectroscopy, Rev. Mod. Phys. **50**, 667 (1978).
[6] D. C. Yost, A. Matveev, E. Peters, A. Beyer, T. W. Hänsch, and Th. Udem, Quantum interference in two-photon frequency-comb spectroscopy, Phys. Rev. A **90**, 012512 (2014).
[7] P. Fendel, S. D. Bergeson, Th. Udem, and T. W. Hansch, Two-photon frequency comb spectroscopy of the 6S-8S transition in cesium, Opt. Lett. **32**, 701 (2007).
[8] R. W. Boyd, *Nonlinear Optics* (Academic Press, San Diego, CA, 1992), p. 105.
[9] T. H. Yoon, A. Marian, J. L. Hall, and J. Ye, Phase-coherent multilevel two-photon transitions in cold Rb atoms: Ultrahigh-resolution spectroscopy via frequency-stabilized femtosecond laser, Phys. Rev. A **63**, 011402(R) (2000).
[10] Photline Inc., Model NIR-MPX800-LN-10-P-P-FA-FA.
[11] S. Schilt, L. Thevenaz, and P. Robert, Wavelength modulation spectroscopy: combined frequency and intensity laser modulation, Appl. Opt. **42**6728 (2003).
[12] P. Meystre and M. Sargent III, *Elements of Quantum Optics*, 3rd ed. (Springer, Berlin, 1998), Chap. 5.4.
[13] E. D. Black, An introduction to Pound-Drever-Hall laser frequency stabilization, Am. J. Phys. **69**, 79 (2001).
[14] C.-Y. Cheng, C.-M. Wu, G.-B. Liao, and W.-Y. Cheng, Cesium $6S_{1/2} \rightarrow 8S_{1/2}$ two-photon transition stabilized 822.5 nm diode laser, Opt. Lett. **32**, 563 (2007).
[15] W.-Y. Cheng, T.-H. Wu, S.-W. Huang, S.-Y. Lin, and C.-M. Wu, Stabilizing the frequency of femtosecond Ti:sapphire comb laser by a novel scheme, Appl. Phys. B **92**, 13 (2008).
[16] T.-W. Liu, C.-M. Wu, Y.-C. Hsu, and W.-Y. Cheng, Dual Ti:sapphire comb lasers by a fiber-laser pumping scheme and a hand-sized optical frequency reference, Appl. Phys. B **117**, 699 (2014).
[17] Y.-Y Chen, T.-W. Liu, C.-M. Wu, C.-C. Lee, and W.-Y. Cheng, High-resolution ^{133}Cs 6S-6D, 6S-8S two-photon spectroscopy using an intracavity scheme, Opt. Lett. **36**, 76 (2011).
[18] D. Touahri, O. Acef, A. Clairon, J. J. Zondy, R. Felder, L. Hilico, B. de Beauvoir, F. Biraben, and F. Nez, Frequency measurement of the $5S_{1/2}(F = 3)-5D_{5/2}(F = 5)$ two-photon transition in rubidium, Opt. Commun. **133**, 471 (1997).
[19] G. Hagel, C. Nesi, L. Jozefowski, C. Schwob, F. Nez, and F. Biraben, Accurate measurement of the frequency of the 6S-8S two-photon transitions in cesium, Opt. Commun. **160**, 1 (1999).
[20] Cesium cells 2, 3, and 0 were all bought from Thorlab Inc.
[21] Th. Udem (private communication).
[22] N. Allard and J. Keilkopf, The effect of neutral nonresonant collisions on atomic spectral lines, Rev. Mod. Phys. **54**, 1103 (1982).
[23] N. D Zameroski, G. D Hager, C. J Erickson, and J. H Burke, Pressure broadening and frequency shift of the $5S_{1/2} \rightarrow 5D_{5/2}$ and $5S_{1/2} \rightarrow 7S_{1/2}$ two photon transitions in ^{85}Rb by the noble gases and N_2, J. Phys. B **47**, 225205 (2014).